



# Practical interpretation of pressure tests of hydraulically fractured vertical wells with finite-conductivity in naturally fractured oil and gas formations

Kittiphong Jongkittinarukorn<sup>1</sup> · Freddy Humberto Escobar<sup>2</sup> · Diana Manuela Ramirez<sup>2</sup> · Daniel Suescún-Díaz<sup>3</sup>

Received: 21 April 2021 / Accepted: 25 June 2021 / Published online: 2 July 2021  
© The Author(s) 2021

## Abstract

This paper presents a well test interpretation methodology using characteristic points and lines found on the pressure and pressure derivative versus time log–log plot for the characterization of a finite-conductivity fractured vertical hydrocarbon well in a double-porosity (heterogeneous) formation considering a new and practical analytical Laplacian model which require less computational time and have more accuracy than semi-analytical models. Some existing equations are found to work well for the new model, and new expressions are developed. The accuracy of the developed equations is successfully tested with synthetical examples.

**Keywords** TDS Technique · Heterogeneous reservoirs · Fractured wells · Bilinear flow · Bi-radial flow

## Abbreviations

$B$	Oil volume factor, bbl/STB
$C$	Wellbore storage coefficient, bbl/psi
$C_{fD}$	Dimensionless hydraulic fracture conductivity
$c_t$	Total system compressibility, MPa <sup>-1</sup>
$h$	Reservoir thickness, ft
$k_{fb}$	Fracture network permeability, md
$k_{fwf}$	Hydraulic fracture conductivity, md-ft
$m(P)$	Pseudopressure, psi <sup>2</sup> /cp
$P$	Pressure, psi
$P_i$	Initial reservoir pressure, psi
$q$	Oil flow rate, BPD
$q_{sc}$	Gas flow rate, Mcsf/D
$s$	Laplacian parameter
$S$	Skin factor
$S'$	Apparent skin factor (gas wells)
$T$	Temperature, °R

$t$	Drawdown time, hr
$t^*\Delta P'$	Pressure derivative, psi
$t^*m(P)'$	Pseudopressure derivative, psi <sup>2</sup> /cp
$t_D$	Dimensionless time, hr
$t_D^*P_D'$	Dimensionless pressure derivative
$tD^*m(P)D'$	Dimensionless pressure derivative, psi
$x_f$	Half-hydraulic fracture length

## Greeks

$\Delta$	Change, drop
$\phi$	Porosity, fraction
$\lambda$	Interporosity flow coefficient
$\mu$	Viscosity, cp
$\omega$	Storativity ratio

## Suffices

$BL$	Bilinear flow regime
$BL1$	Bilinear flow regime read at $t = 1$ h
$BR$	Bi-radial flow regime
$BR1$	Bi-radial flow regime read at $t = 1$ h
$D$	Dimensionless
$Dxf$	Dimensionless based on fracture length
$f$	Hydraulic fractured
$f+m$	Natural fractures + matrix
$g$	Gas
$i$	Initial
$ma$	Matrix
$min$	Minimum
$nf$	Fracture network

✉ Freddy Humberto Escobar  
fescobar@usco.edu.co

<sup>1</sup> Department of Mining and Petroleum Engineering, Chulalongkorn University, Patumwan, Bangkok 10330, Thailand

<sup>2</sup> Department of Petroleum Engineering, Universidad Surcolombiana, Avenida Pastrana, Neiva (Huila), Colombia

<sup>3</sup> Departamento de Ciencias Naturales, Universidad Surcolombiana, Avenida Pastrana, Neiva (Huila), Colombia

$r_1$	Radial flow regime before the trough
$r_2$	Radial flow regime after the trough
$u_s$	Unit-slope during trough
$u_{si}$	Intercept of unit-slope with radial flow lines

## Introduction

More than half of the world's hydrocarbon reserves are stored in naturally fractured occurring formations which many times require hydraulic fracturing to enhance fluid production. These two issues: (1) naturally fractured reservoirs and (2) hydraulically fractured wells were originally separated from the well testing point of view. On one hand, the most classical paper on naturally fractured reservoirs was introduced by Warren and Root (1963) who presented a model to study the characteristic behavior of a porous medium possessing a network of fractures. They also introduce two key concepts: the interporosity flow parameter and the storativity ratio. On the other hand, Gringarten and Ramey (1973) made use of the Green's function to introduce a mathematical model to describe the pressure behavior of a well with an infinite-conductivity fracture. This solution opened a new frontier in the field of well test analysis. Later, an excellent contribution to this field was made by Cinco-Ley et al. (1976). They provided an semi-analytical solution to study the pressure behavior of a vertical well intercepted by a finite-conductivity fracture. Besides, they also defined the onset value of the dimensionless fracture conductivity to establish whether a fracture falls into a finite-conductivity or infinite-conductivity classification.

Cinco-Ley and Meng (1988) built a bridge between fractured wells and naturally fractured formations by introducing a very practical Laplacian analytical solution to describe the pressure behavior of these combine systems. This solution is also used in this work for comparison purposes. Several other important solutions have also been introduced, even including trilinear model. Finally, Wei et al. (2021) just introduced some very practical Laplacian solutions for finite-conductivity fractures which possess small differences with the solution provided Cinco-Ley and Meng (1988) and are worth of providing an interpretation technique which is the matter of this paper.

As it is well known, both transient rate and pressure analysis are important tools for reservoir characterization and adequate interpretation of those is also important for field appraisal and decision making. As commented by Escobar et al. (2018), there exists four ways of well pressure and rate data interpretation: (1) Type curve-matching, (2) Conventional straight-line, (3) Nonlinear regression analysis (computer assisted) and (4) TDS Technique. The last one can be found with detail in the books by Escobar (2015, 2019). This method uses characteristic points and lines found on

the pressure derivative or reciprocal rate derivative versus time log-log plot from which analytical and direct-forward expressions are employed to find reservoir parameters. The very first paper on this technique was presented by Tiab (1993) for homogeneous infinite reservoirs, followed by Tiab (1994) for uniform-flux and infinite-conductivity hydraulic fractured wells and Tiab et al. (1999) for infinite-conductivity vertical fractured wells.

There are two noticeable differences between the pressure traces generated by the models of Wei et al. (2021) and Cinco-Ley and Meng (1988): (1) For dimensionless fracture conductivity ( $C_{fD}$ ) less than 3, the first one does not display the classical trough during the transition period found on naturally fractured formations, and only bilinear flow is observed. For  $C_{fD} > 3$ , a bilinear flow regime is first observed then a trough interrupts the bilinear flow regime, but a bi-radial (elliptical) flow regime follows and, later, the radial flow regime is again interrupted by a trough. (2) The second model always has the trough during early bilinear flow regime, and another bilinear flow regime follows the trough. There is no trough during radial flow regime. Thereby, the objective of this work is to provide an interpretation technique for the model of Wei et al. (2021) applicable to both oil and gas wells (Appendix A). Some existing expressions presented by Engler and Tiab (1996), Tiab and Bettam (2007) and Escobar et al. (2015) were found to work here, and other were developed and successfully tested with synthetical and real examples.

## Mathematical formulation

Wei et al. (2021) presented a novel and practical analytical well pressure solutions for finite-conductivity fractured wells in naturally occurring formations. This model considers the following assumptions: (1) The fracture is symmetrical around the wellbore and it possesses constant values of height, half-fracture length, width and permeability. (2) Fluid enters the wellbore only through the finite-conductivity fracture. (3) The matrix systems with a permeability,  $k_{ma}$ , porosity,  $\phi_{ma}$ , and comprehensive compressibility,  $c_{ma}$ , bears a single and slightly compressible and constant viscosity fluid,  $\mu$ . (3) the fracture network has a permeability,  $k_{mf}$ , porosity,  $\phi_{mf}$ , comprehensive compressibility,  $c_{mf}$  has a single-phase fluid with viscosity,  $\mu$ . (4) The fluid obeys Darcy's law, negligible gravity and capillary force. The Warren-Root model is used to describe the naturally fractured system, then, natural fractures are assumed to be uniformly distributed. Reservoir properties over the entire domain are identical. Therefore, the reservoir is a homogeneous dual-porosity system with bulk permeability,  $k_{fb}$ . (5) The well produces at a constant rate.

Cinco-Ley and Meng (1988) presented a general semi-analytical solution for finite-conductivity fractured wells in dual-porosity reservoirs. They were also based on Warren-Root considerations which means that the physical model and assumptions are essentially the same. However, Wei et al. (2021) stated that semi-analytical or numerical solutions are the most used for pressure-transient analysis for finite-conductivity fractured wells in naturally fractured reservoir now. However, these just mentioned solutions are time-consuming and easily encounter some computation problems, such as accuracy, convergence and stability. The solution proposed by Wei et al. (2021) contains infinite series resulting in calculation times much shorter and simpler than the semi-analytical and numerical solutions presented in the literature, including the one presented by Cinco-Ley and Meng (1988).

The Laplacian infinite constant rate solution of Wei et al. (2021), which neglects wellbore storage effects, is given below:

$$\bar{P}_D(s) = \frac{\pi}{s\sqrt{2C_{fD}}\sqrt[4]{sf(s)} \tanh\left[\sqrt{\frac{2}{C_{fD}}}\sqrt[4]{sf(s)}\right]} - \frac{\pi}{2s\sqrt{sf(s)}} + \frac{0.4063}{s\left(C_{fD} + 0.8997 + \frac{1.6252}{\pi}sf(s)\right)} + \frac{1}{2s} \int_{-1}^1 K_0\left(\sqrt{(0.372 - \alpha)^2 sf(s)}\right) d\alpha \tag{1}$$

where  $f(s)$  is given by:

$$f(s) = \omega + \frac{(1 - \omega)\lambda}{(1 - \omega)s + \lambda} \tag{2}$$

The dimensionless fracture storativity ratio is given by

$$\omega_f = \frac{(\phi c_i)_f}{(\phi c_i)_{f+m}} \tag{3}$$

And the dimensionless matrix interporosity coefficient is:

$$\lambda = \alpha x_f^2 \frac{k_{ma}}{k_{fb}} \tag{4}$$

Being  $\alpha$  the shape parameter which depends upon the matrix surface area and block type. The dimensionless time, based on half-fracture length, is given below:

$$t_{Dxf} = \frac{0.000263k_{fb}t}{(\phi c_i)_{f+m}\mu x_f^2} \tag{5}$$

The dimensionless pressure and pressure derivative parameters for oil reservoirs are given by:

$$P_D = \frac{k_{fb}h\Delta P}{141.2q\mu B} \tag{6}$$

$$t_D * P'_D = \frac{k_{fb}h(t * \Delta P')}{141.2q\mu B} \tag{7}$$

The dimensionless fracture conductivity introduced by Cinco-Ley et al. (1976) is defined as:

$$C_{fD} = \frac{k_f w_f}{k_{fb} x_f} \tag{8}$$

### Pressure response

As observed in Fig. 1, there exist certain differences between the model of Wei et al. (2021) and the one presented by Cinco-Ley and Meng (1988). Although, substantially, both

pressure behaviors are about the same, it is noticeable in the plot that the Cinco-Ley and Meng model presents bilinear flow regime before and after the characteristic transition displayed by naturally fractured reservoirs which consists of a trough. On the other hand, the model by Wei et al., matter of this study, presents bilinear flow regime before the trough but bi-radial or elliptical, Tiab (1994), flow regime

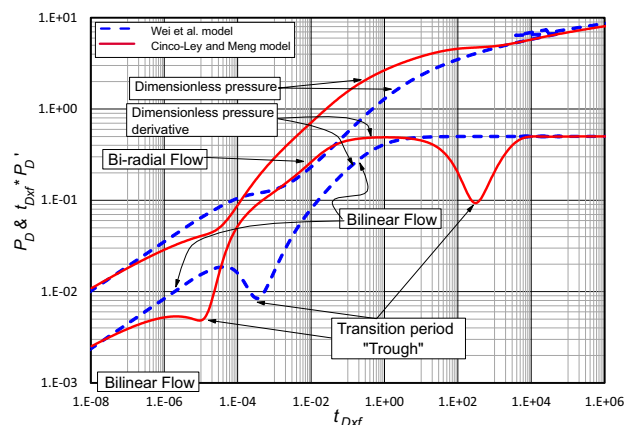


Fig. 1 Dimensionless pressure and pressure derivative versus dimensionless time using the models of Wei et al. (2021) and Cinco-Ley and Meng (1988) when  $\lambda_m = 5 \times 10^{-4}$ ,  $C_{fD} = 20$  and  $\omega = 0.05$

after the trough. This flow regime is characterized by a 0.36-slope on the pressure derivative curve. However, referring to Figs. 2 and 3, the mentioned situation occurs when  $C_{fD}$  is greater than 3 (the plot shows for  $C_{fD} = 5$ ). Below this value, the bilinear flow is not interrupted by the trough. It is also noticeable that the model of Wei et al. always displays a trough during radial flow regime, but the Cinco-Ley and Meng model does not has this characteristic.

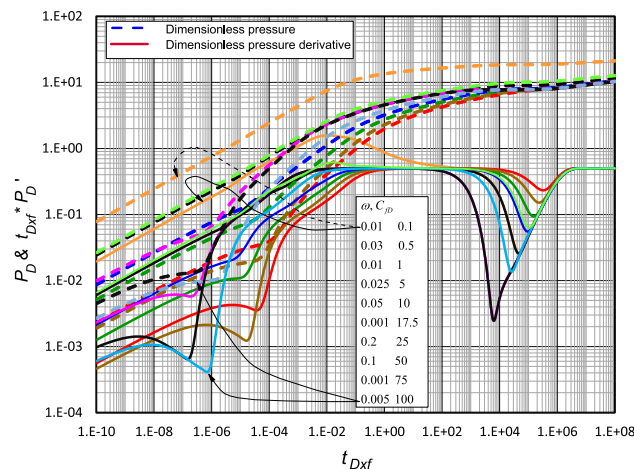
The authors believe that the pressure response given by the model of Wei et al. (2021) is realistic since there is a trough for conductivity higher than 3 which indicates than the more conductive the fracture the more possibility of depleting the fluid inside the fracture, although partially; therefore, the final fracture network depletion takes place during the radial flow regime. The model by Cinco-Ley and Meng (1988) acts as if the fracture network feeding the hydraulic fracture were fully depleted before the radial flow regime shows up.

Figure 4 attempts to provide a better understanding of the system domain. The hydraulic fracture is fed by fracture network. Once they are depleted, the matrix feeds the fracture network and either bilinear, elliptical or radial flow follow that process.

### Interpretation methodology

Some of the equations presented by Tiab and Bettam (2007) and Escobar et al. (2015) do not work in the model of Wei et al. (2021); therefore, some of the provided equations must be modified, and other new equations must be developed.

The interpretation methodology applied here follows the philosophy of the TDS Technique, Tiab (1993); therefore, unified pressure derivative behaviors should be obtained to



**Fig. 2** Dimensionless pressure and pressure derivative versus dimensionless time for  $\lambda_m = 1 \times 10^{-6}$  and different values of  $C_{fD}$  and  $\omega$

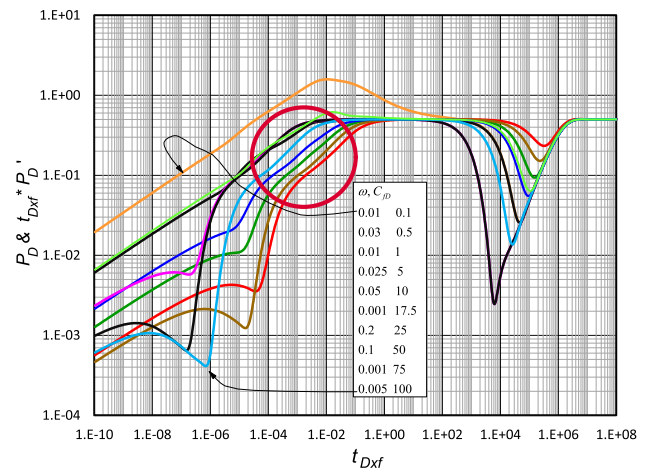


**Fig. 3** Dimensionless pressure derivative versus dimensionless time for  $\lambda_m = 1 \times 10^{-6}$  and different values of  $C_{fD}$  and  $\omega$

develop analytical expressions for the determination of the reservoir parameters. Such is the case presented in Fig. 5 in which the early bilinear flow regime has a unified behavior which allowed us to obtain the pressure and pressure derivative governing equations which were also reported by Tiab and Bettam (2007):

$$P_D = \frac{2.451}{\sqrt{C_{fD}}} \left( \frac{t_{Dxf}}{\omega} \right)^{1/4} \tag{9}$$

$$t_{Dxf} * P'_D = \frac{0.6127}{\sqrt{C_{fD}}} \left( \frac{t_{Dxf}}{\omega} \right)^{1/4} \tag{10}$$

As seen, the pressure behavior depends simultaneously upon both dimensionless fracture conductivity and

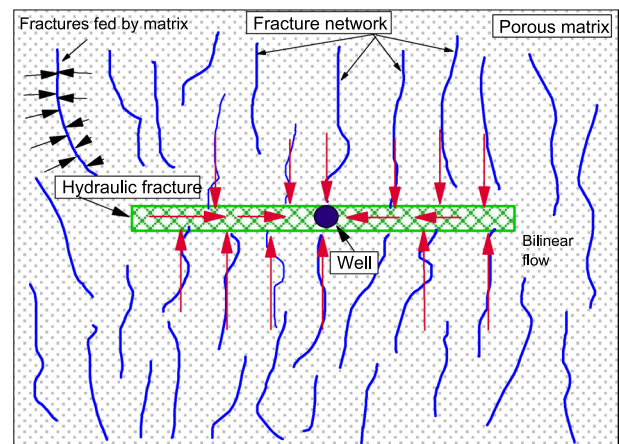


**Fig. 4** Schematic representation of the studied domain

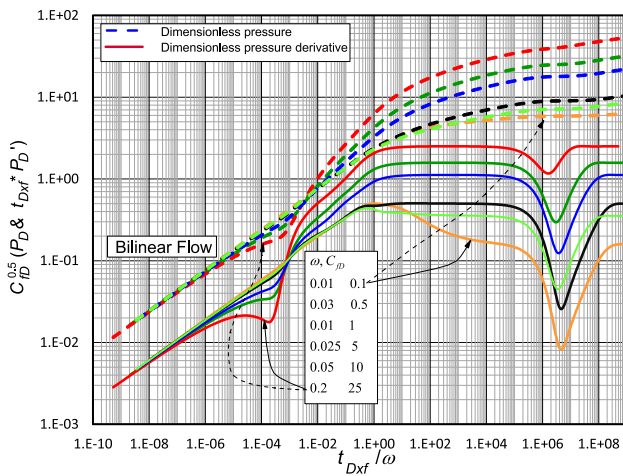


**Fig. 5** Unified dimensionless pressure and pressure derivative versus dimensionless time divided by  $\omega$  during bilinear flow regime

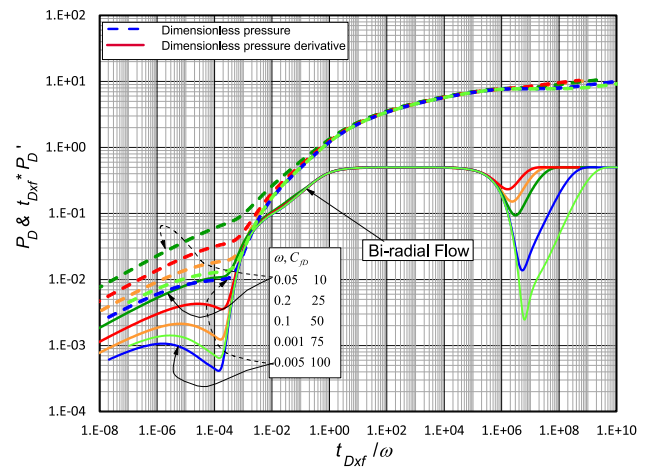


**Fig. 6** Unified dimensionless pressure and pressure derivative versus dimensionless time divided by  $\omega$  during bi-radial flow regime

dimensionless storativity ratio. Therefore, it was difficult to find a governing behavior during the trough since, at early time, the trough does not move neither to the right implying an independence from the interporosity flow parameter.

Solving for the fracture conductivity from Eqs. (9) and (10) led to:

$$k_f w_f = \frac{1947.46}{\sqrt{\omega \mu (\phi c_t)_{f+m} k_{fb} t_{BL}}} \left( \frac{q \mu B}{h(\Delta P)_{BL}} \right)^2 \tag{11}$$

$$k_f w_f = \frac{121.74}{\sqrt{\omega \mu (\phi c_t)_{f+m} k_{fb} t_{BL}}} \left( \frac{q \mu B}{h(t * \Delta P)'_{BL}} \right)^2 \tag{12}$$

When the pressure derivative is too noisy, it is recommended to draw the most representative line over the given flow regime and read the pressure derivative value at the time of 1 h. This also helps to have the best averaged value. Under this condition, Eqs. (11) and (12) became:

$$k_f w_f = \frac{121.74}{\sqrt{\omega \mu (\phi c_t)_{f+m} k_{fb}}} \left( \frac{q \mu B}{h(t * \Delta P)'_{BL1}} \right)^2 \tag{13}$$

$$k_f w_f = \frac{1947.46}{\sqrt{\omega \mu (\phi c_t)_{f+m} k_{fb}}} \left( \frac{q \mu B}{h(\Delta P)_{BL1}} \right)^2 \tag{14}$$

Another unified behavior was found in Fig. 6, this time, during bi-radial flow regime. However, the dimensionless pressure does not follow a parallel straight-line behavior along with the pressure derivative curve; so only a pressure derivative governing equation was developed for this flow

regime, and it was also found that the developed expression coincided with the one reported by Escobar et al. (2015):

$$t_{Dxf} * P'_D = \left( \frac{\pi t_{Dxf}}{26\xi} \right)^{0.36} \tag{15}$$

It is worth to mention that the pressure behavior in Escobar et al. (2015) does go parallel to the pressure derivative curve, but it does not in the model of Wei et al. (2021).

Solving for the half-fracture length from Eq. (15), it yielded:

$$x_f = 5.4595 \left( \frac{qB}{h(t * \Delta P)'_{BR}} \right)^{1.3889} \sqrt{\frac{t_{BR}}{\omega (\phi c_t)_{f+m} \left( \frac{\mu}{k_{fb}} \right)^{1.778}}} \tag{16}$$

Again, sometimes it is better to read the value at the time of 1 h; then, Eq. (16) became:

$$x_f = 5.4595 \left( \frac{qB}{h(t * \Delta P)'_{BR1}} \right)^{1.3889} \sqrt{\frac{1}{\omega (\phi c_t)_{f+m} \left( \frac{\mu}{k_{fb}} \right)^{1.778}}} \tag{17}$$

Before going further, during the bi-radial flow regime the dimensionless fracture conductivity no longer affects this flow, but the dimensionless fracture storativity ratio does. As observed in the circled zone of Fig. 3, there exists a relationship between the bi-radial flow regime pressure derivative and the dimensionless fracture storativity ratios which was found to be:

$$\omega = \sqrt{0.3457 - 0.22982 \ln \left( \frac{kh(t * \Delta P)'_{BR1}}{141.2q\mu B} \right)} \tag{18}$$



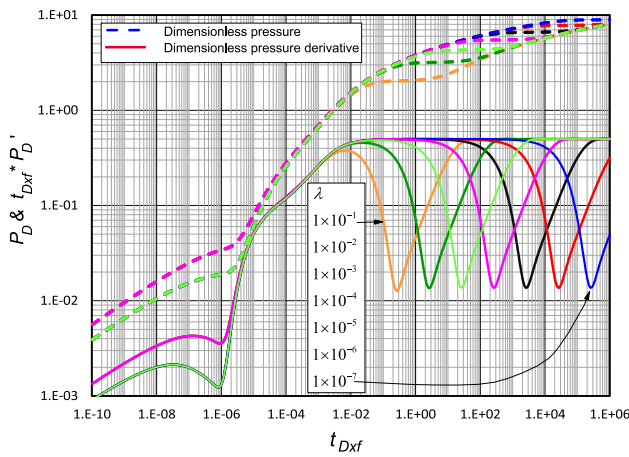


**Fig. 7** Dimensionless pressure and pressure derivative versus dimensionless time for by  $\omega=0.005$  and different  $\lambda_m$  values

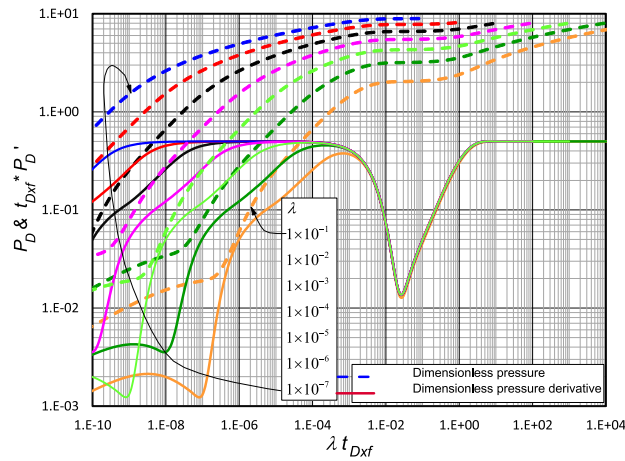


**Fig. 8** Unified dimensionless pressure and pressure derivative versus dimensionless time multiplied by  $\lambda_m$  for  $\omega=0.005$  and different  $\lambda_m$  values

Figure 7 shows the effect of the interporosity flow coefficient on the pressure test. Figure 8 displays a normalized behavior of the same case when both pressure and pressure derivative were multiplied by the interporosity flow coefficient. In this case, a unified unit-slope line and a minimum point are unique. They obey the following mathematical behavior:

$$t_{Dxf} * P'_D = 0.4774 \lambda t_{Dxf} \tag{19}$$

$$\lambda (t_{Dxf})_{\min} = 0.026303 \tag{20}$$

After plugging, the dimensionless time given by Eq. (5) into Eq. (19) yielded an expression for the estimation of the interporosity flow coefficient.

$$\lambda = \frac{99.745 \mu (\phi c_t)_{f+m} x_f^2}{k_{fb} t_{\min}} \tag{21}$$

Replacement of the dimensionless time, Eq. (5), and dimensionless pressure derivative definition, Eq. (7), into Eq. (19) led to find another expression to calculate the interporosity flow coefficient using any arbitrary point during the unit-slope pseudosteady-state period during the transition period or trough:

$$\lambda = \frac{(\phi c_t)_{f+m} x_f^2 h (t * \Delta P')_{us}}{56.27 q B t_{us}} \tag{22}$$

Tiab (1993) established that during the radial flow regime, the dimensionless pressure derivative is governed by the following straight-line equation:

$$t_D * P'_D = 0.5 \tag{23}$$

The intersection between Eqs. (19) and (23) also led to find another expression to find the interporosity flow coefficient:

$$\lambda = \frac{3971.71 \phi \mu c_r x_f^2}{k_{fb} t_{usi}} \tag{24}$$

### Other expressions

The authors found that some expressions given by Engler and Tiab (1996), Tiab and Bettam (2007) and Escobar et al. (2015) can be used here changing the wellbore radius by the half-fracture length. The following equations also applied here:

$$\omega = 0.15866 \left\{ \frac{(t * \Delta P')_{\min}}{(t * \Delta P')_r} \right\} + 0.54653 \left\{ \frac{(t * \Delta P')_{\min}}{(t * \Delta P')_r} \right\}^2 \tag{25}$$

$$\omega = 0.19211 \left\{ \frac{5 t_{\min}}{t_{b2}} \right\} + 0.80678 \left\{ \frac{5 t_{\min}}{t_{b2}} \right\}^2 \tag{26}$$

$$\lambda = \left[ \frac{42.5 h (\phi c_t)_{f+m} x_f^2}{q B_o} \right] \frac{(t * \Delta P')_{\min}}{t_{\min}} \tag{27}$$

Tiab and Escobar (2003) also presented an equation for the determination of the interporosity flow coefficient from using the minimum point during the trough in the pressure derivative plot or the inflection point during the transition on the semilog plot.

$$\lambda = \frac{3792\mu(\phi c_t)_{f+m} x_f^2}{k_{fb} t_{min}} \left[ \omega \ln \left( \frac{1}{\omega} \right) \right] \quad (28)$$

Engler and Tiab (1996) also presented expressions to find permeability and skin factor in naturally fractured formations:

$$k_{fb} = \frac{162.2q\mu B}{h(t * \Delta P')_{r1,r2}} \quad (29)$$

$$S = \frac{1}{2} \left[ \left( \frac{\Delta P}{t * \Delta P'} \right)_{r1} - \ln \left( \frac{k_{fb} t_{r1}}{(\phi c_t)_{f+m} \mu r_w^2 \omega} \right) + 7.43 \right] \quad (30)$$

$$S = \frac{1}{2} \left[ \left( \frac{\Delta P}{t * \Delta P'} \right)_{r2} - \ln \left( \frac{k_{fb} t_{r2}}{(\phi c_t)_{f+m} \mu r_w^2 \omega} \right) + 7.43 \right] \quad (31)$$

Refer to Appendix A to find equations for gas wells.

### Examples

#### Synthetic example 1

Synthetic test data were generated using data from the second column of table 1 and reported in Fig. 9. As observed in that plot, only bilinear flow is observed before the radial flow regime, and the transition period only interrupts the radial flow regime. From such plot, the following information was read:

**Table 1** Input data for the example

Parameter	Synthetic Example1	Synthetic Example2	Field example
$k_{fb}$ , md	100	300	
$h$ , ft	100	120	65.62
$r_w$ , ft		0.328	
$q$ , bbl/D	120	380	377
$B$ , rb/STB	1.34	1.2	1.144
$\mu$ , cp	0.75	3.2	2.242
$x_f$ , ft	100	300	215.511
$(\phi)_{f+m}$	0.18	0.1	0.1
$(c_t)_{f+m}$ , 1/psi	$1 \times 10^{-6}$	$1.8 \times 10^{-6}$	$1.21 \times 10^{-6}$
$\Omega$	0.01	0.05	
$\Lambda$	$1 \times 10^{-5}$	$1 \times 10^{-6}$	
$k_f w_f$ , md-ft	1000	1,350,000	
$C_{fD}$	0.1	20	

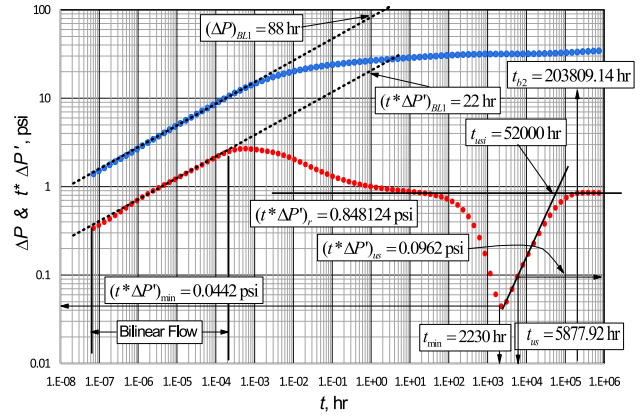


**Fig. 9** Pressure and pressure derivative versus time for synthetic example 1

$(t * \Delta P')_r = 0.848124 \text{ psi}$      $t_{min} = 2230 \text{ h}$   
 $(t * \Delta P')_{BL1} = 22 \text{ psi}$      $(t * \Delta P')_{min} = 0.0442 \text{ psi}$   
 $t_{b2} = 203809.13 \text{ h}$      $(\Delta P)_{BL1} = 88 \text{ psi}$   
 $t_{usi} = 52000 \text{ h}$      $t_{us} = 5877.92 \text{ h}$   
 $(t * \Delta P')_{us} = 0.096 \text{ psi}$

Use Eq. (29) to find fracture network permeability:

$$k_{fb} = \frac{70.6(120)(0.75)(1.34)}{(100)(0.848124)} = 100.390 \text{ md}$$

The hydraulic fracture conductivity is found by using Eqs. (13) and (14):

$$k_f w_f = \frac{121.74}{\sqrt{(0.01)(0.75)((0.18)(1 \times 10^{-6})(100.390))}} \left( \frac{(120)(0.75)(1.34)}{(100)(22)} \right)^2 = 995.670 \text{ md - ft}$$

$$k_f w_f = \frac{1947.46}{\sqrt{(0.01)(0.75)((0.18)(1 \times 10^{-6})(100.390))}} \left( \frac{(120)(0.75)(1.34)}{(100)(88)} \right)^2 = 995.476 \text{ md - ft}$$

Use Eqs. (24), (27) and (28) to calculate the interporosity flow coefficient:

$$\lambda = \frac{3971.71(0.75)((0.18)(1 \times 10^{-6})(100^2))}{(100.390)(52000)} = 1.027 \times 10^{-6}$$

$$\lambda = \left[ \frac{42.5(100)((0.18)(1 \times 10^{-6})(100^2))}{(120)(1.34)} \right] \frac{0.044198}{2230} = 9.34 \times 10^{-7}$$

$$\lambda = \frac{3792(0.75)(0.18)(1 \times 10^{-6})(100^2)}{(100.390)(2230)}$$

$$\left[ (0.01) \ln \left( \frac{1}{0.01} \right) \right] = 1.053 \times 10^{-6}$$

The dimensionless fracture storativity ratio with Eqs. (25) and (26).

$$\omega = 15866 \left\{ \frac{(0.044198)}{(0.848124)} \right\} + 0.54653 \left\{ \frac{(0.044198)}{(0.848124)} \right\}^2 = 0.0975$$

$$\omega = 0.19211 \left\{ \frac{5(2230)}{203809.13} \right\} + 0.80678 \left\{ \frac{5(2230)}{203809.13} \right\}^2 = 0.0129$$

## Synthetic example 2

Pressure and pressure derivative versus time data reported in Fig. 10 were generated with the information provided in the third column of Table 1. It can be observed in this plot that there exists bilinear flow regime before the trough and bi-radial flow regime after the trough. The following information was read from Fig. 10:

$$(t * \Delta P')_r = 02.865 \text{ psi} \quad t_{\min} = 9471.83 \text{ h}$$

$$(t * \Delta P')_{BL1} = 2.13 \text{ psi} \quad (t * \Delta P')_{\min} = 0.536 \text{ psi}$$

$$t_{b2} = 260875.69 \text{ h} \quad (\Delta P)_{BL1} = 8.5 \text{ psi}$$

$$t_{usi} = 65000 \text{ h} \quad t_{us} = 19789.45 \text{ h}$$

$$(t * \Delta P')_{us} = 0.7752 \text{ psi} \quad (t * \Delta P')_{BR1} = 9 \text{ psi}$$

Fracture network permeability and hydraulic fracture conductivity were estimated with Eqs. (29), (13) and (14), respectively:

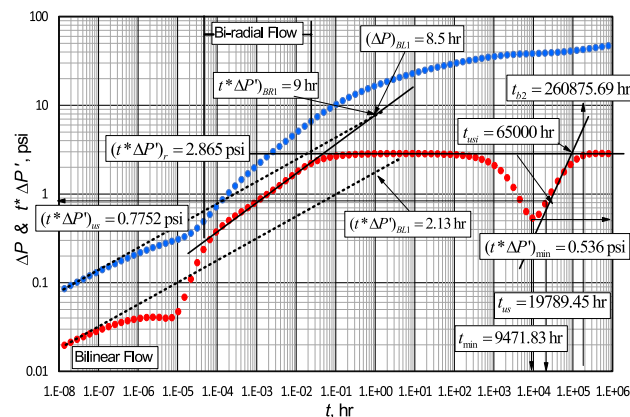


**Fig. 10** Pressure and pressure derivative versus time for synthetic example 2

$$k_{fb} = \frac{70.6(380)(3.2)(1.2)}{(120)(2.864)} = 299.649 \text{ md}$$

$$k_f w_f = \frac{121.74}{\sqrt{(0.05)(3.2)(0.1)(1.8 \times 10^{-6})(299.649)}}$$

$$\left( \frac{(380)(3.2)(1.2)}{(120)(2.130)} \right)^2 = 1349846.5 \text{ md} \cdot \text{ft}$$

$$k_f w_f = \frac{1947.46}{\sqrt{(0.05)(3.2)((0.1)(1.8 \times 10^{-6})(299.64)}}$$

$$\left( \frac{(380)(3.2)(1.2)}{(120)(8.5)} \right)^2 = 1355941.6 \text{ md} \cdot \text{ft}$$

The half-fracture length was determined with Eq. (17) to be:

$$x_f = 5.4595 \left( \frac{(380)(1.2)}{(120)(9)} \right)^{1.3889}$$

$$\sqrt{\frac{1}{(0.05)(0.1)(1.9 \times 10^{-6})} \left( \frac{3.2}{300} \right)^{1.778}} = 306.805 \text{ ft}$$

The interporosity flow parameter was calculated using Eqs. (21), (22), (24), (27) and (28):

$$\lambda = \frac{99.745(3.2)(0.1)(1.8 \times 10^{-6})(300^2)}{300(9471.83)} = 1.82 \times 10^{-6}$$

$$\lambda = \frac{56.27(0.1)(1.8 \times 10^{-6})(300^2)(120)(0.775)}{(380)(1.2)(19789.4447)} = 9.39 \times 10^{-6}$$

$$\lambda = \frac{3971.71(3.2)(0.1)(1.8 \times 10^{-6})(300^2)}{(299.649)(65000)} = 1.057 \times 10^{-5}$$

$$\lambda = \left[ \frac{42.5(120)(0.1)(1.9 \times 10^{-6})(300^2)}{(3.2)(1.2)} \right]$$

$$\frac{0.535}{9471.823} = 1.025 \times 10^{-5}$$

$$\lambda = \frac{3792(3.2)(0.1)(1.8 \times 10^{-6})(300^2)}{(299.649)(9471.823)}$$

$$\left[ (0.05) \ln \left( \frac{1}{0.05} \right) \right] = 1.037 \times 10^{-5}$$

Find the dimensionless fracture storativity ratio with Eqs. (25) and (26).

$$\omega = 0.15866 \left\{ \frac{0.535}{2.864} \right\} + 0.54653 \left\{ \frac{0.535}{2.864} \right\}^2 = 0.0487$$



$$\omega = 0.19211 \left\{ \frac{5(9471.82)}{260875.69} \right\} + 0.80678 \left\{ \frac{5(9471.82)}{260875.69} \right\}^2 = 0.0614$$

The dimensionless fracture storativity ratio can also be obtained from the elliptical flow regime by using the value of the pressure derivative at 1 h into Eq. (18):

$$\omega = \left[ 0.3457 - 0.22982 \ln \left( \frac{(300)(120)(9)}{141.2(380)(3.2)(1.2)} \right) \right]^2 = 0.0584$$

### Field example

Wei et al. (2021) presented a field example which was solved by their model and the model by Cinco-Ley and Meng (1988). Pressure and pressure derivative versus time data were digitized and reported in Fig. 11. Relevant information for this test is reported in the fourth column of Table 1.

As observed in Fig. 11, pressure data are too noisy at early time, and bilinear flow regime is unidentified, but bi-radial flow regime can be seen between about 0.01 and 3 h. The following characteristic points were read from Fig. 11:

$$\begin{aligned} (t * \Delta P')_r &= 89.67 \text{ psi} & t_{\min} &= 69.3 \text{ h} \\ (t * \Delta P')_{BR1} &= 87 \text{ psi} & (t * \Delta P')_{\min} &= 46.6 \text{ psi} \\ t_{b2} &= 69.3 \text{ h} \end{aligned}$$

Permeability was estimated with Eq. (29):

$$k_{fb} = \frac{70.6(377)(2.242)(1.144)}{(65.62)(89.67)} = 11.601 \text{ md}$$

Use the value of the pressure derivative during bi-radial flow at 1 h to find half-fracture length using Eq. (17) and the dimensionless fracture storativity ratio with Eq. (25):

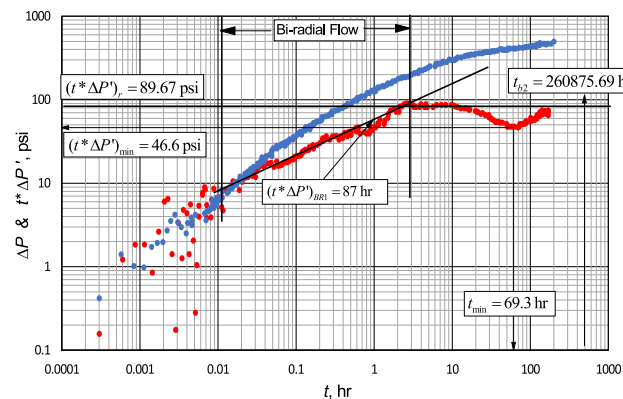


Fig. 11 Pressure and pressure derivative versus time for field case

$$x_f = 5.4595 \left( \frac{(377)(1.144)}{(65.62)(87)} \right)^{1.3889} \sqrt{\frac{1}{(0.230)(0.1)(1.21 \times 10^{-6})} \left( \frac{2.242}{11.601} \right)^{1.778}} = 209.964 \text{ ft}$$

$$\omega = 0.15866 \left\{ \frac{46.6}{89.67} \right\} + 0.54653 \left\{ \frac{46.6}{89.67} \right\}^2 = 0.23$$

Find the interporosity flow parameter with Eq. (21):

$$\lambda = \frac{99.745(0.1)(2.242)(1.21 \times 10^{-6})(209.964^2)}{(11.601)(69.3)} = 0.00148$$

### Final comments

According to the obtained results from the worked examples, TDS Technique can reproduce the reservoir parameters in a practical and accurate way as seen from the examples of the given model for a finite-conductivity hydraulically fractured well in a heterogeneous (naturally fractured) formation.

In spite the data were digitized in the field example, Table 2 indicates that the results from the actual field case agree quite well with those from previous estimations by Wei et al. (2021) and Cinco-Ley and Meng (1988) who used either nonlinear regression analysis or type curve-matching since they mentioned the word matching and do not provide any analytical methodology.

The simulated examples results are summarized in Table 3. As it can be observed there, the reservoir parameters are estimated from several sources, and the results agree very well with the input data used for the simulations.

### Conclusions

New expressions for the characterization of well pressure tests are obtained for finite-conductivity fractured wells draining naturally fractured occurring formations for a model presented by Wei et al. (2021). Also, some existing equations were slightly modified to adjust to this model.

Table 2 Comparison of field example results

Parameter	Wei et al (2021)	Cinco-Ley and Meng	This work
$k_{fb}$ , md	9.686	9.6	11.6
$\Omega$	0.198	0.19	0.23
$\Lambda$	0.00136	0.00131	0.0015
$x_f$ , md-ft	216.5	213.2	209.97

**Table 3** Comparison of synthetic example results

Parameter	Eq	Calculated Value	Original value
<i>Synthetic example 1</i>			
$k_{fb}$ , md	29	100.4	100
$\Lambda$	24	$1.03 \times 10^{-6}$	$1 \times 10^{-6}$
	27	$9.34 \times 10^{-7}$	
	28	$1.05 \times 10^{-6}$	
$\Omega$	25	0.098	0.01
	26	0.013	
$k_{fw}$ , md-ft	13	995.7	1000
	1	995.5	
<i>Synthetic example 2</i>			
$k_{fb}$ , md	29	299.7	300
$\lambda$	21	$1.82 \times 10^{-6}$	$1 \times 10^{-5}$
	22	$9.4 \times 10^{-6}$	
	24	$1.06 \times 10^{-5}$	
	27	$1.03 \times 10^{-5}$	
	28	$1.04 \times 10^{-5}$	
$\omega$	25	0.049	0.05
	26	0.061	
	18	0.059	
$k_{fw}$ , md-ft	13	1,349,846.5	1,135,000
	14	1,355,941.6	
$x_f$ , md-ft	17	306.8	300

The equations are successfully validated with synthetic and field examples.

The model of Cinco-Ley and Meng (1988) always presents the transition period caused by the fluid depletion inside the hydraulic fracture during the bilinear flow regime, also a bilinear flow regime follows once the transition period vanishes. The model by Wei et al. (2021) does not display transition period when the dimensionless fracture conductivity is less than 3. Above this value, a transition period interrupts the bilinear flow regime and bi-radial (elliptical) flow regime follows the transition, and another transition takes place during linear flow regime, meaning that the hydraulic fracture did not fully deplete the natural fracture network during the early time.

The first transition period does not allow to find reservoir parameters since it depends on both dimensionless fracture conductivity and dimensionless fracture storativity ratio. When, bi-radial flow dominates the pressure behavior, dimensionless fracture conductivity no longer affects the pressure behavior, and it is possible to find an expression to correlate between the dimensionless fracture storativity ratio and the value of the pressure derivative during this period which was extrapolated to its reading at 1 h.

## Appendix

### Appendix A- Gas flow equations

The dimensionless time, pseudopressure and pseudopressure quantities are defined by:

$$t_{Dxf} = \frac{0.000263k_{fb}t}{(\phi c_i)_{f+m}\mu x_f^2} \quad (32)$$

$$m(P)_D = \frac{hk[m(P_i) - m(P)]}{1424.52q_{sc}T} \quad (33)$$

$$t_D * m(P)'_D = \frac{hk[t * \Delta m(P)']}{1424.52q_{sc}T} \quad (34)$$

Recently, Nguyen et al. (2020) remarked on the lacking of linearization due to the retaining pressure-dependent viscosity-compressibility in fracture wells in unconventional gas reservoirs. Such effect was also noticed by Escobar et al. (2012) who found some discrepancies when estimating the hydraulic fracture and naturally fracture parameters when using pseudotime and rigorous time.

To overcome the above issue, Agarwal (1979) introduced the pseudotime function to account for the time dependence of gas viscosity and total system compressibility:

$$t_a = \int_{t_0}^t \frac{dt}{\mu(t)c_i(t)} \quad (35)$$

Pseudotime is better defined as a function of pressure as a new function given in hr psi/cp:

$$t_a(P) = \int_{P_0}^P \frac{(dt/dP)}{\mu(P)c_i(P)} dP \quad (36)$$

Including the pseudotime function,  $t_a(P)$ , in Eq. (32), the dimensionless pseudotime is given by:

$$t_{Da} = \left( \frac{0.0002637k}{\phi x_f^2} \right) t_a(P) \quad (37)$$

Notice that the viscosity-compressibility product is not seen in Eq. (37), since they are included in the pseudotime function. However, if we multiply and, then, divide by  $(\mu c_i)_i$  a similar equation to the general dimensionless time expression, Eq. (37), will be obtained.

$$t_{Da} = \left( \frac{0,0002637k}{\phi(\mu c_t)_{f+m} r_w^2} \right) \{ [\mu(c_t)_{f+m}] \times t_a(P) \} \quad (38)$$

The equivalence of Eqs. (11) and (12) are:

$$k_f w_f = \frac{197960.6}{\sqrt{\omega(\phi)_{f+m} k_{fb} t_a(P)_{BL}}} \left( \frac{q_{sc} T}{h(\Delta P)_{BL}} \right)^2 \quad (39)$$

$$k_f w_f = \frac{12370.52}{\sqrt{\omega(\phi)_{f+m} k_{fb} t_a(P)_{BL}}} \left( \frac{q_{sc} T}{h(t * \Delta P)'_{BL}} \right)^2 \quad (40)$$

The equivalence to Eqs. (16) and (18) are:

$$x_f = 138.687 \left( \frac{q_{sc} T}{h(t * \Delta m(P)')_{BR}} \right)^{1.3889} \sqrt{\frac{t_a(P)_{BR}}{\omega(\phi)_{f+m} k^{1.778}}} \quad (41)$$

$$\omega = \sqrt{0.3457 - 0.22982 \ln \left( \frac{hk[t * \Delta m(P)']_{BR1}}{1424.52 q_{sc} T} \right)} \quad (42)$$

The equivalence to Eq. (22) and (27) are:

$$\lambda = \frac{(\phi)_{f+m} x_f^2 h [t * \Delta m(P)']_{us}}{5.577 q_{sc} T t_a(P)_{us}} \quad (43)$$

$$\lambda = \left[ \frac{4.218 h (\phi)_{f+m} x_f^2}{qT} \right] \frac{[t * \Delta m(P)']_{\min}}{t_a(P)_{\min}} \quad (44)$$

The equivalence to Eqs. (29)-(31) are:

$$k = \frac{711.26 qT}{h[t * \Delta m(P)']_r} \quad (45)$$

$$S' = 0.5 \left[ \frac{[\Delta m(P)]_{r1}}{[t * \Delta m(P)']_{r1}} - \ln \left( \frac{k t_a(P)_{r1}}{(\phi)_{f+m} r_w^2 \omega} \right) + 7.4316 \right] \quad (46)$$

$$S' = 0.5 \left[ \frac{[\Delta m(P)]_{r2}}{[t * \Delta m(P)']_{r2}} - \ln \left( \frac{k t_a(P)_{r2}}{(\phi)_{f+m} r_w^2} \right) + 7.4316 \right] \quad (47)$$

Equations (21), (24), (25) (26) and (28) apply to gas reservoirs after dropping the viscosity-compressibility term and replace time by pseudotime. Care must be taking when using Eq. (26) since a change for the pressure derivative by the pseudopressure derivative must be made.

## Declarations

**Conflict of interest** On behalf of all the co-authors, the corresponding author states that there is no conflict of interest.

**Ethical statement** This manuscript has not be submitted to other journal for simultaneous consideration. The submitted work is original and has not been published elsewhere in any form or language (partially or in full). This study is not split up into several parts to increase the quantity of submissions and submitted to various journals or to one journal over time. Results are presented clearly, honestly and without fabrication, falsification or inappropriate data manipulation (including image-based manipulation). Authors adhere ourselves to discipline-specific rules for acquiring, selecting and processing data. No data, text or theories by others are presented as if they were the author's own ('plagiarism'). Proper acknowledgements to other works must be given (this includes material that is closely copied (near verbatim), summarized and/or paraphrased), quotation marks (to indicate words taken from another source) are used for verbatim copying of material, and permissions secured for material that is copyrighted.

**Open Access** This article is licensed under a Creative Commons Attribution 4.0 International License, which permits use, sharing, adaptation, distribution and reproduction in any medium or format, as long as you give appropriate credit to the original author(s) and the source, provide a link to the Creative Commons licence, and indicate if changes were made. The images or other third party material in this article are included in the article's Creative Commons licence, unless indicated otherwise in a credit line to the material. If material is not included in the article's Creative Commons licence and your intended use is not permitted by statutory regulation or exceeds the permitted use, you will need to obtain permission directly from the copyright holder. To view a copy of this licence, visit <http://creativecommons.org/licenses/by/4.0/>.

## References

- Agarwal RG (1979) "Real gas pseudo-time" - A new function for pressure buildup analysis of MHF gas wells. doi: <https://doi.org/10.2118/8279-MS>.
- Cinco-Ley H, Meng HZ (1988) Pressure transient analysis of wells with finite conductivity vertical fractures in double porosity reservoirs. In: Paper presented at the SPE Annual Technical Conference and Exhibition, Houston, Texas, October 1988. doi: <https://doi.org/10.2118/18172-MS>.
- Cinco-Ley H, Samaniego F, Dominguez N (1976) Transient pressure behavior for a well with a finity-conductivity vertical fracture. In: Paper SPE 6014 presented at the SPE-AIME 51st annual fall technical conference and exhibition, held in New Orleans, LA, October 3–6.
- Engler T, Tiab D (1996) Analysis of pressure and pressure derivative without type curve matching, 4 Naturally fractured reservoirs. J Petrol Sci Eng 15:127–138
- Escobar FH (2015) Recent advances in practical applied well test analysis. Nova publishers New York. Published by Nova Science Publishers, Inc. † New York. 423p. Nov.
- Escobar FH (2019) Novel, integrated and revolutionary well test interpretation analysis. IntechOpen Mind, England. 278p. doi: <https://doi.org/10.5772/intechopen.81078>. ISBN 978-1-78984-850-2 (print). ISBN 978-1-78984-851-9 (online).
- Escobar FH, Martinez LY, Méndez LJ, Bonilla LF (2012) Pseudo-time application to hydraulically fractured vertical gas wells and

- heterogeneous gas reservoirs using the TDS technique. *J Eng Appl Sci* 7(3):260–271
- Escobar FH, Zhao YL, Fahes M (2015) Characterization of the naturally fractured reservoir parameters in infinite-conductivity hydraulically-fractured vertical wells by transient pressure analysis. *J Eng Appl Sci* 10(12):5352–5362
- Escobar FH, Jongkitnarukorn K, Hernandez CM (2018) The power of TDS technique for well test interpretation: a short review. *J Petroleum Explor Prod Technol*. <https://doi.org/10.1007/s13202-018-0517-5>
- Gringarten AC, Ramey HJ (1973) The use of source and green's functions in solving unsteady-flow problems in reservoirs. *SPE J* 13:285–296. <https://doi.org/10.2118/3818-PA>
- Nguyen KH, Zhang M, Ayala LF (2020) Transient pressure behavior for unconventional gas wells with finite-conductivity fractures. *Fuel* 266:117119. <https://doi.org/10.1016/j.fuel.2020.117119>
- Tiab D (1993) Analysis of pressure and pressure derivative without type-curve matching: 1- skin and wellbore storage. *J Petrol Sci Eng* 12:171–181
- Tiab D (1994) Analysis of pressure and pressure derivative without type curve matching: vertically fractured wells in closed systems. *J Petrol Sci Eng* 11:323–333
- Tiab D, Bettam Y (2007) Practical interpretation of pressure tests of hydraulically fractured wells in a naturally fractured reservoir. In: Paper presented at the Latin American & Caribbean petroleum engineering conference, Buenos Aires, Argentina, April. doi:<https://doi.org/10.2118/107013-MS>
- Tiab D, Escobar FH (2003) Determinación del Parámetro de Flujo Interporoso a Partir de un Gráfico Semilogarítmico". X Congreso Colombiano del petróleo. Oct. 14–17. ISBN 958-33-8394-5. Bogotá (Colombia).
- Tiab D, Azzougen A, Escobar FH, Berumen S (1999) Analysis of pressure derivative data of finite-conductivity fractures by the "Direct Synthesis" technique. 1999. In: Paper presented at the SPE mid-continent operations symposium, Oklahoma City, Oklahoma, March. doi: <https://doi.org/10.2118/52201-MS>
- Warren JE, Root PJ (1963) The Behavior of Naturally Fractured Reservoirs. *SPE J* 3:245–255. <https://doi.org/10.2118/426-PA>
- Wei C, Chenga S, Shi W, Yua H (2021) Practical pressure-transient analysis solutions for a well intercepted by finite conductivity vertical fracture in naturally fractured reservoirs. *J Petroleum Sci Eng*. Volume 204, September 2021, Article number 108768.

**Publisher's Note** Springer Nature remains neutral with regard to jurisdictional claims in published maps and institutional affiliations.